

Numerical Simulation of Wideband Calorimeter for High Power Microwave

Ivan K. Kurkan^{*}, Alexey I. Klimov, Pavel V. Pripitnev, and Vladislav V. Rostov

Abstract—The novel design of an ultra-wideband calorimeter for energy measurement of high power microwave pulses of nanosecond duration is proposed in this paper. The main idea is the use of a circular waveguide with losses in the wall and metal cone insertion at the axis to increase attenuation constant in the waveguide. The efficiency of the concept was proved with the numeric simulation and optimization of the calorimeter design with ANSYS HFSS software for frequencies from 8 to 38 GHz. The operating modes are supposed to be symmetric TM_{0n} ones. Ethanol was chosen as an absorbing medium. It is parted from the vacuum volume by a plastic tube. The frequency dependencies of ethanol's relative permittivity and loss tangent were taken into account in the simulation model. The reflection coefficient for TM_{01} mode is below -20 dB at the lowest frequency of 8 GHz and well below the level of -25 dB from 10 to 38 GHz. The reflection coefficients for higher order modes remain below -30 dB until the operating frequency is close to the cut-off frequency for a particular mode. The maximum accepted power level is of hundreds of megawatts for pulses of a nanoseconds duration. The effect of waveguide modes mixture at the input of the calorimeter on the maximum accepted power level was considered. This level may differ by 4 times between specific modes mixtures. Therefore, the transition from a particular microwave source to the calorimeter input should be carefully optimized.

1. INTRODUCTION

The high power microwave (HPM) pulses generation [1] is of great interest over the past decades, and it drives such fields as directed energy, space propulsion, and high-power radar. An important characteristic of such pulses is microwave power amplitude, which can vary widely and exceed the level of one gigawatt [2, 3]. It is generally recognized that the most reliable method for amplitude determination is associated with measuring the energy and microwave pulse envelope (power vs. time). The pulse energy is measured with microwave calorimeters [4–22], and microwave detectors [18, 23, 24] incorporated in the measurement circuit can be used to record the waveform of microwave radiation power. The operation of the microwave calorimeter is based on microwave energy dissipation in the material of the absorbing load of the calorimeter and the measurement of this dissipated energy in a certain way. Two types of calorimeters are mostly used in relativistic microwave electronics: “dry” [4–10] and liquid [11–22] ones. The design of a “dry” calorimeter includes a solid medium with optimal dimensions and shape for absorbing microwave radiation. An increase in its temperature is measured with thermistors or thermocouples to quantify the absorbed energy. In the design of a liquid calorimeter, a radiolucent dielectric volume with optimal geometric characteristics filled with a liquid medium is usually used. Either the temperature increase or the increase in the volume of the liquid due to absorption of microwave energy is measured. In the latter case, the load casing must have sufficient rigidity.

Received 11 November 2019, Accepted 2 April 2020, Scheduled 6 May 2020

^{*} Corresponding author: Ivan K. Kurkan (ikk@lfe.hcei.tsc.ru).

The authors are with the Institute of High Current Electronics (IHCE) SD RAS, Akademicheskoy Ave. 2/3, Tomsk 634055, Russia.

Calorimeters can be either broadband or narrowband, designed to use with a specific microwave source. The calibration of “dry” calorimeters requires a precision source of microwave pulses with pre-defined (or accurately measured) pulse energy. In contrast, in liquid calorimeters, the calibration can be performed by applying an electric pulse with a known energy to a resistive load located inside the volume of the absorbing fluid.

At a relatively low power of the microwave pulse, calorimeters [4–9, 11–14] of rather small transverse dimensions are used. With a power increase, a microwave discharge can occur in such a load, similar to a discharge along the window surface of a horn antenna of a powerful source of microwave radiation [25, 26]. Therefore, at high power, calorimeters with increased transverse dimensions of an absorbing load, which are weakly sensitive to the mode composition of microwave radiation, are used [15–22]. The input window of the disk-shaped load of the liquid calorimeter can be corrugated to reduce the reflection of incident waves [22]. Such a load can be mounted to the opening of the transmitting horn antenna [18] or placed in front of the antenna aperture [19]. A noticeable problem when using calorimeters with disk-shaped absorbing loads is the diffraction power losses of microwave radiation, causing a power leak through the gap between the opening of the transmitting antenna and the load [27, 28]. This problem is avoided in the case of a dry calorimeter [10] with the absorbing load based on a circular waveguide of the diameter that is much larger than the wavelength. In this design, microwave energy is absorbed by elements made of a special radio-absorbing material placed on the inner cylindrical surface of the waveguide. This kind of calorimeters is weakly sensitive to the mode composition of the radiation. The incident waves are reflected by the metal cone placed inside the waveguide to the absorbing wall. The absorbed energy is determined from the temperature increment of the absorber measured with thermocouples. As noted above, the calibration procedure for such a calorimeter is more complicated and requires a special source of microwave pulses with known energy. Dry loaded calorimeters are also known to require rather long time of more than 10 s to reach the thermal equilibrium between absorbing medium and thermosensitive elements.

Since the cylindrical geometry can provide the necessary structural rigidity, it is of interest to study the feasibility of implementing a calorimeter of a similar design, but with an absorber that uses ethanol-based operating fluid, which has well established in wide-aperture disk-shaped loads (see in [12, 19] as an exmpl.). Thus, the main idea of the proposed calorimeter design with a closed type load is the use of a cylindrical waveguide with losses in the outer wall. The load is to be connected to the output waveguide of the microwave pulse source by a special conical transition. The absorbing fluid is separated from the vacuum volume by a dielectric tube. This work is devoted to numerical simulation and optimization of the absorbing load of such liquid calorimeter with ANSYS HFSS [29] to be used in ultra wideband, namely, from X to Ka-band.

The paper is organized as follows. In Section 2, the task definition including some technical requirements and discussion on used materials as well as the numerical simulation method and concept design are introduced. Section 3 represents the results of simulation: electric fields and microwave losses spatial distributions, reflection coefficients for symmetric TM_{0n} modes in the band of 8–38 GHz. The importance of the careful design of transition from an HPM oscillator to the calorimeter is also considered here.

2. TASK DEFINITION AND SIMULATION METHOD

Absorption of microwaves in waveguide walls was taken as a core idea of the closed type calorimeter design. In contrast to partially filled with lossy medium waveguides and wide-aperture (obstacle-like) calorimeters, the proposed design provides perfect matching in a wide band. The 95% ethanol is supposed to be used as the lossy medium, since it has proved its feasibility in other designs [12–16, 18, 19, 21]. Ethanol and a vacuum volume are parted by a dielectric tube. The calorimeter design should provide the high electric field strength to accept the microwave input power of hundreds of megawatts. The microwave breakdown level for such short pulses is above the commonly used level of 30 kV/cm for pulses of tens nanoseconds. The breakdown level of 37 kV/cm was experimentally obtained for the microwave pulse duration of about ten nanoseconds at microwave output window in the research [30]. One of the reasons of this breakdown level increase is that the multipactor discharge needs a few tens or more nanoseconds to develop [31, 32]. Therefore, we assume the electric field strength

of 60 kV/cm as the maximum for microwave pulses of a few nanoseconds duration. Symmetric TM_{0n} modes are supposed to be operating ones. The operating frequency band should start in X-band and cover all bands, including Ka-band at least. The reflection coefficient should not exceed the level of -20 dB within the operating band.

To meet the parameters declared above, a lot of constraints should be applied on a dielectric material used in design. At first, it should have chemical resistance to ethanol. The electric permittivity should be relatively low (namely below 2.5) to prevent electric field enhancement at the vacuum-dielectric interface. The loss tangent should be as low as possible. As we are about to measure an increase in the liquid volume, a dielectric should provide mechanical stability of the calorimeter in operating. High-density polyethylene and polypropylene random copolymer (PPRC) meet the stated demands. The latter one was finally chosen as a wide range of PPRC tubes for water supply are commercially available. It should be the pure material without a dye or prints on its surface, which affect the dielectric properties. The real part of polypropylene's dielectric permittivity is constant within considered frequency band, and the dielectric loss tangent is of the order of 10^{-4} (three orders less than that for ethanol) [33]. Thus, in simulations we used constant relative permittivity and zero losses for dielectric material.

It was difficult to get precise data on ethanol dielectric properties above the frequency of 15 GHz because they were represented in large-scale graphs [34–36]. However, we have the experimental data for 95% ethanol in the band of 1 to 15 GHz, which were obtained at the Department of Radioelectronics of the Tomsk State University using PNA E8363B network analyzer (Agilent Technologies) according to the technique [37] with the use of a small-size coaxial probe from the Dielectric Probe Kit 85070E. These data were used for interpolation to the higher frequency band by Cole-Cole model [38]. It is so-called single exponent model, but it gives acceptable error level up to about 40 GHz [36]. The data obtained were added to the HFSS material model as piece-wise functions on frequency for the relative permittivity and the loss tangent of the dielectric. The relative permittivity is weakly varying for frequencies above the 12.5 GHz, and it is close to the value of 4.5. While the loss tangent has three-fold drop from L- to K-band down to the value of about 0.3.

The 3D numerical simulations were carried out with ANSYS HFSS (High Frequency Structure Simulator) using finite-difference frequency-domain (FDFD) method [29]. HFSS uses finite element method (FEM) to solve electrodynamic equations, including adaptive mesh refinement to provide given accuracy. It works on the tetrahedral mesh. Driven Modal design solution type, which provides the multiple modes solution for passive microwave structures, such as waveguides, coaxial and microstrip lines etc., was used in simulations. The results are the set of S -parameters and internal field structure.

As the symmetric TM_{0n} modes were chosen as the operating ones, simulations were conducted on the 10° sector of a cylinder with the Symmetric H Plane boundary conditions applied to planes cutting the sector. Yet the refined mesh size reaches about 600 thousands tetrahedrons to obtain the accuracy level of 2% for S -parameters at the upper frequencies. All outer faces excluding cutting planes and input port have Perfect Electric Conductor (PEC) boundary conditions.

The initial design as a circular waveguide with losses at the wall requires a considerable length to provide the stated level of reflections. It was proposed to add a cone shaped insertion at the axis to transform operating symmetric modes to the quasi-TEM ones that, hence, increased the absorption performance. The chosen input port size was large enough to be overmoded even in the lowest band. It is supposed to use an optimized transition section for a particular microwave source forming a mixture of modes at the input of the calorimeter. The importance of the transition is discussed in the next section.

The size optimization was carried out on input waveguide diameter, absorbing volume, length and taper angle of the cone to minimize exterior dimensions at the given level of input power. Initial optimization was done in K-band, then the model was tested to meet the requirements in X-band and some corrections were made as needed. Optimized design of the calorimeter's absorbing load is shown in Figure 1.

3. SIMULATION RESULTS AND DISCUSSIONS

The electric field strength distributions for the input power level of 400 MW for TM_{01} and TM_{02} modes at 10 GHz and TM_{01} mode at 36.6 GHz are shown in Figures 2–4. The maximum electric field strength

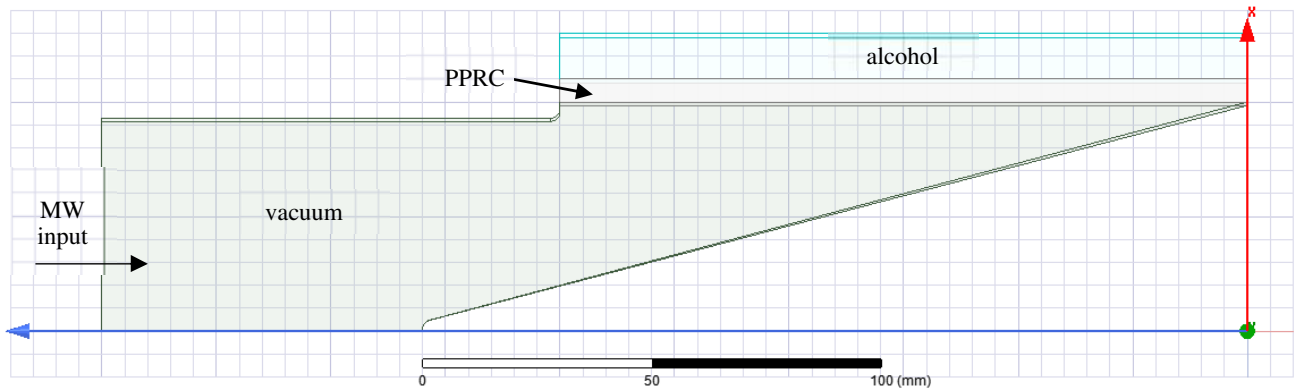


Figure 1. The simulation model of the calorimeter's absorbing load.

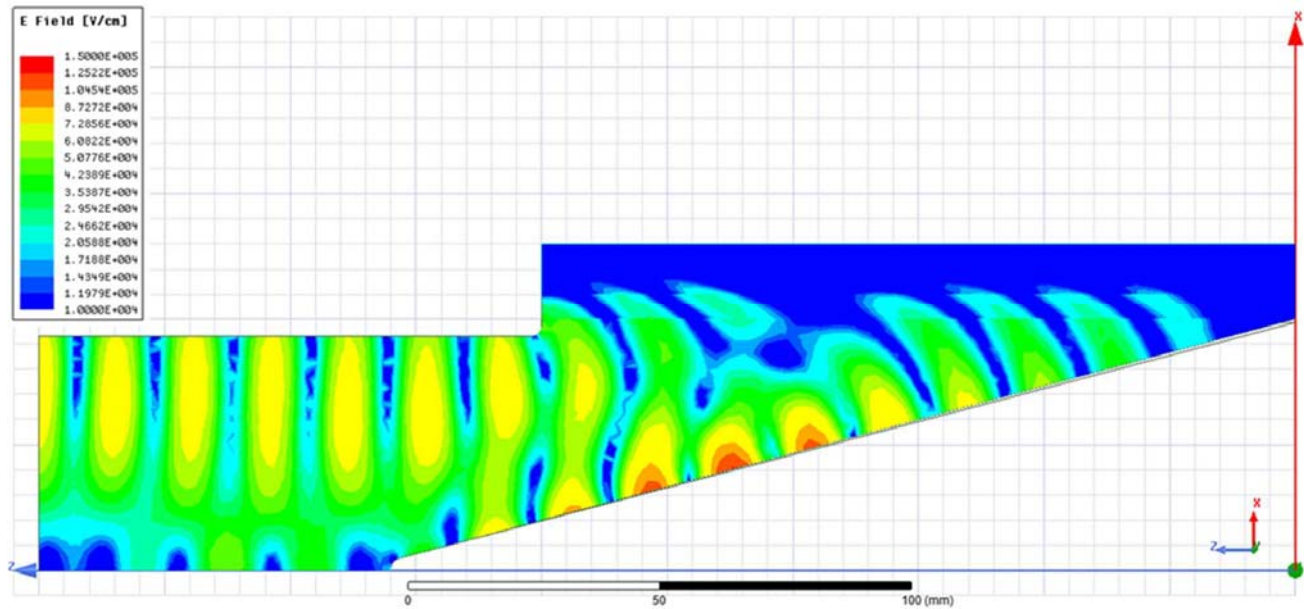


Figure 2. The electric field strength distribution for TM_{01} mode at the input power of 400 MW and frequency of 10 GHz.

is at the cone. Its value is about 150 kV/cm. However, the most critical point, defining the dielectric strength of the calorimeter, is the dielectric-vacuum surface. The normal component of electric field strength measured in Volts per meter at the vacuum-dielectric boundary for the input power of 400 MW for TM_{01} mode at the frequencies of 10 and 36.6 GHz are shown in Figures 5 and 6 respectively. The maximum values are about the level of 45 kV/cm at 36.6 GHz and about 34 kV/cm at 10 GHz. So, the maximum input power for microwave pulses of a few nanoseconds duration can be estimated as 700 MW at 36.6 GHz and over 1 GW at 10 GHz, assuming 60 kV/cm as an allowed maximum of the electric field strength.

Figures 7 and 8 represent the spatial distribution of the volume loss density in the alcohol volume for the input power of 400 MW for TM_{01} mode at the frequencies 10 and 36.6 GHz. The logarithmic scale is used for better representation of the results. The volume loss density at the upper radius of the simulated alcohol volume is more than two orders of magnitude lower than that at the dielectric-liquid surface. Therefore, calibration and thermostabilizing heaters needed in a real calorimeter could be placed in a liquid above this radius with no effect on the electromagnetic fields in the main volume.

After the optimization procedure at fixed frequencies of 36.6 and 10 GHz, wideband simulations

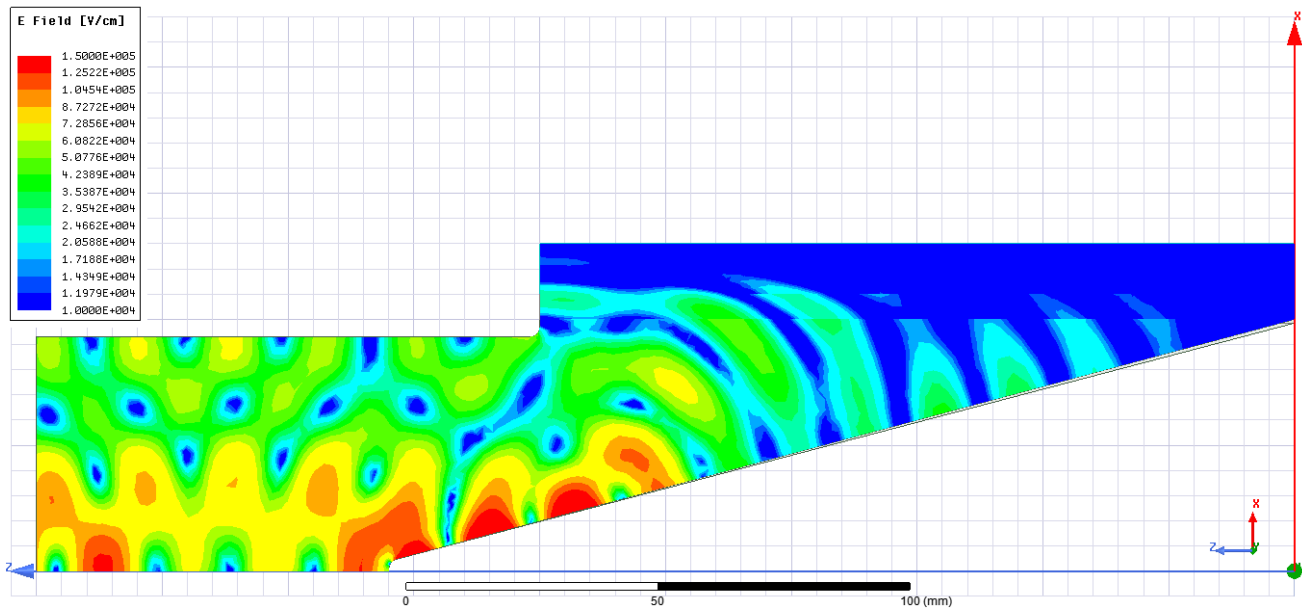


Figure 3. The electric field strength distribution for TM_{02} mode at the input power of 400 MW and frequency of 10 GHz.

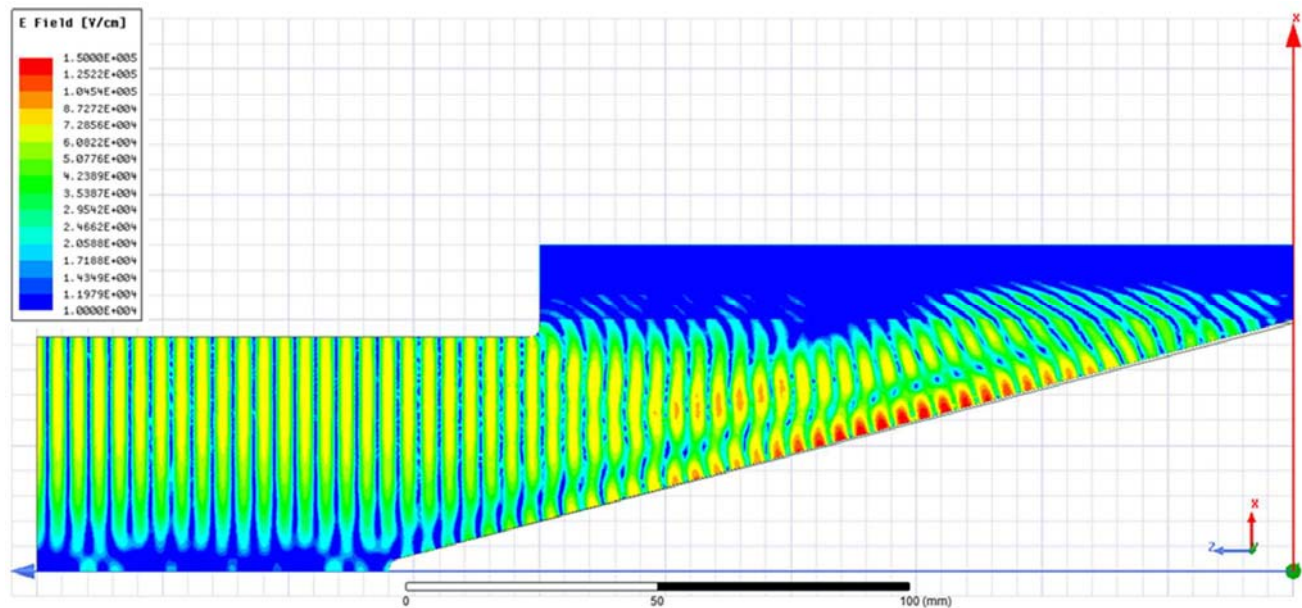


Figure 4. The electric field strength distribution for TM_{01} mode at the input power of 400 MW and frequency of 36.6 GHz.

were conducted from 8 up to 38 GHz using frequency dependent relative permittivity and loss tangent for alcohol. The discreet sweep with 0.2 GHz step with saving field for further post-processing analysis was used. The whole frequency band was divided into 4 subbands to save the calculation time. The adaptive mesh refinement iterations were ran at the highest frequency of every subband until S -parameter error dropped below 2%. Then calculations were carried out within the subband using the obtained fine mesh.

The frequency dependence of reflection coefficients for symmetric TM_{0n} modes is shown in Figure 9. The reflection coefficients of all five symmetric modes reflection (TM_{05} is not shown in the figure for the

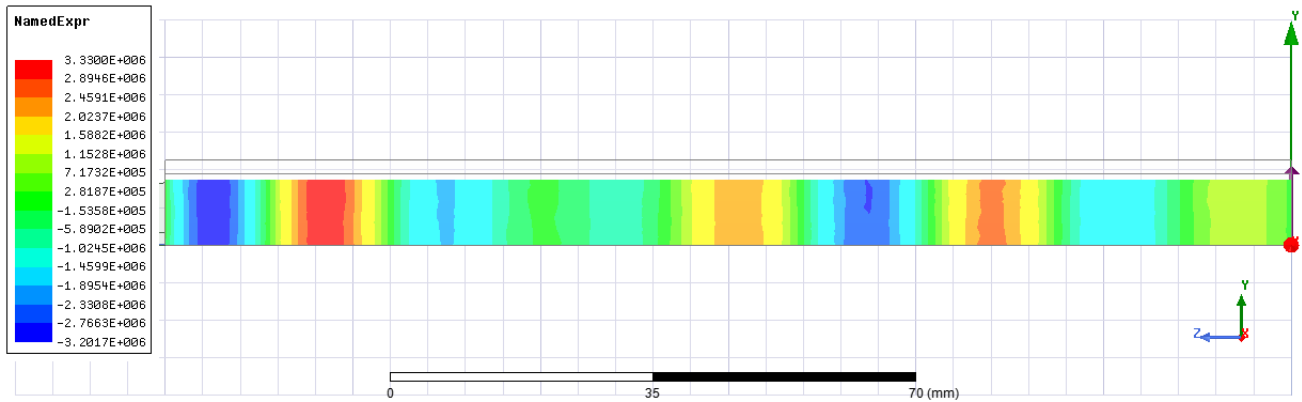


Figure 5. The normal component of the electric field strength [V/m] at the vacuum-dielectric boundary for TM_{01} mode at the input power of 400 MW and frequency of 10 GHz.

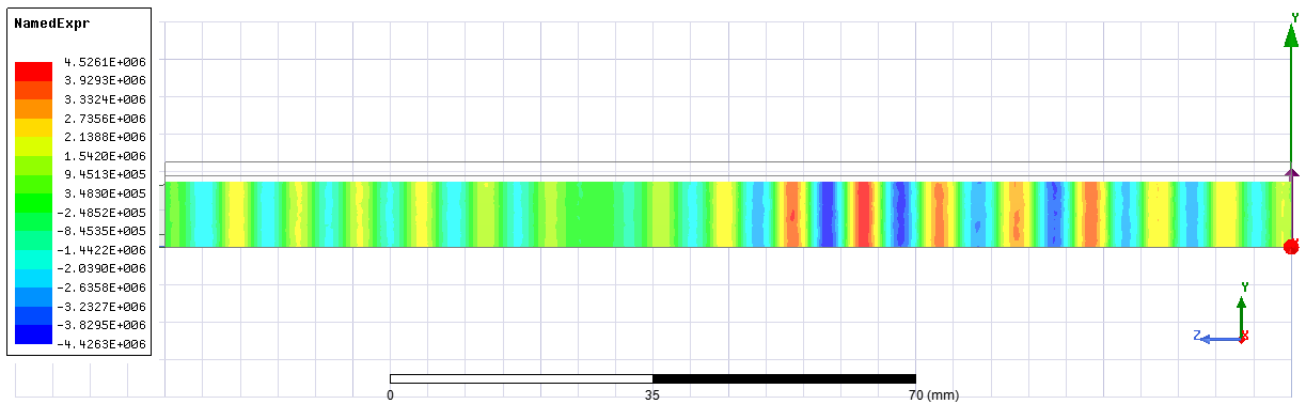


Figure 6. The normal component of the electric field strength [V/m] at vacuum-dielectric boundary for TM_{01} mode at the input power of 400 MW and frequency of 36.6 GHz.

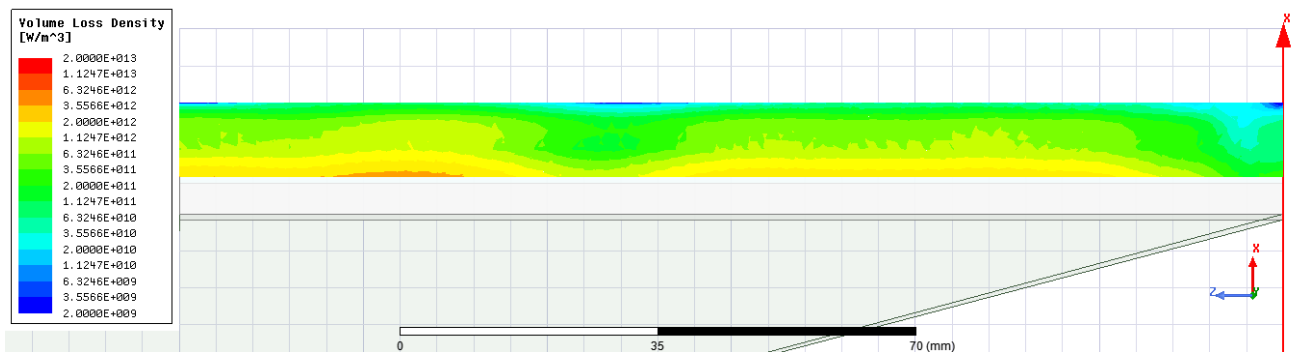


Figure 7. The spatial distribution of the volume loss density in the alcohol volume for TM_{01} mode at the input power of 400 MW and frequency of 10 GHz.

sake of clarity) are below -30 dB in the band of 31–38 GHz. The reflection coefficient increases while approaching the cut-off frequency for the particular mode. The reflection coefficient of TM_{01} mode remains below -20 dB at the lowest frequency.

Figure 10 shows the results obtained with the Field Calculator, which is the built-in option of HFSS for data post processing. These are maxima of normal electric field strength at the dielectric surface in

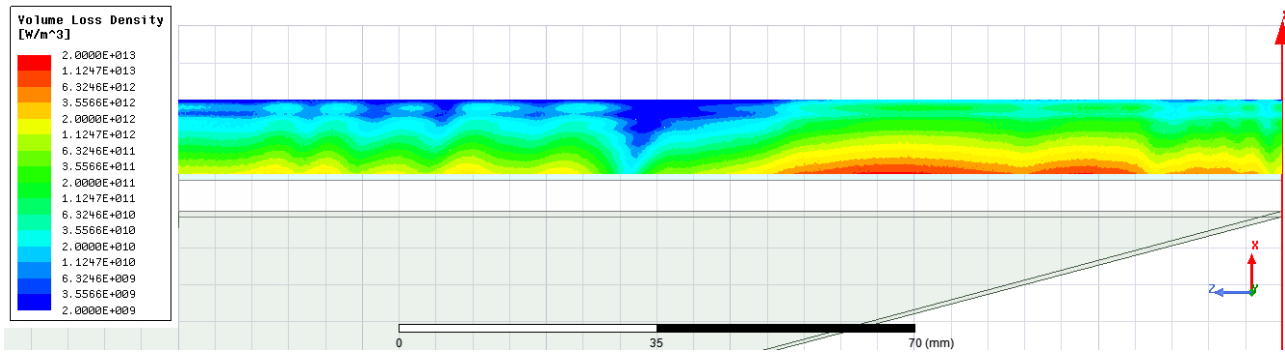


Figure 8. The spatial distribution of the volume loss density in the alcohol volume for TM_{01} mode at the input power of 400 MW and frequency of 36.6 GHz.

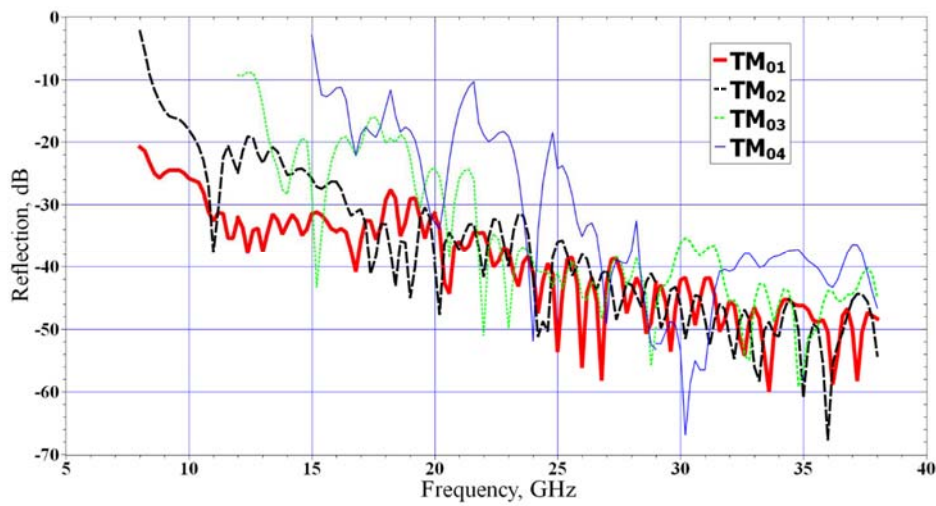


Figure 9. The reflection coefficients for the first four symmetric TM_{0n} modes vs. frequency.

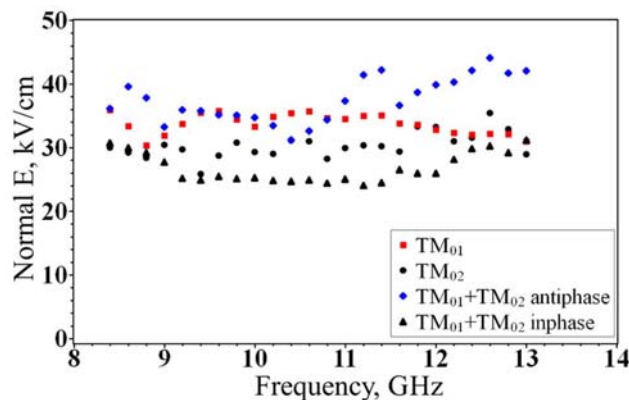


Figure 10. Overall maximum of normal electric field strength on the vacuum side of the dielectric surface for modes TM_{01} , TM_{02} and their mixtures in X-band at the input power of 400 MW.

X-band for TM_{01} and TM_{02} modes as well as for their 50/50 mixtures. The input power level for all cases was 400 MW. The optimization of modes mixture ratio and their phase shifts is out of the scope of this paper. These results are just to demonstrate an option to increase the maximum accepted power

of the calorimeter with the use of an optimized transition section from a particular microwave source to the input of the calorimeter. Moreover, a careless design of transition might result in the microwave breakdown in the calorimeter at the input power level that is much less than the expected one. One can see that the electric field strength between antiphase and in phase mixtures $TM_{01} + TM_{02}$ differs by the factor of two at certain frequencies. Hence, the maximum accepted power for the antiphase mixture might be four times lower than that for the in phase one.

Finally, we would like to mention that this concept design could be scaled up and down and easily modified for a coaxial input of power. To accept more input power, the dimensions of the absorbing load should be increased. The enlarged inner radius of the dielectric decreases the electric field strength on its surface. The length of the load should be sufficient to adsorb the whole incident power. There are two options to lower the minimal operating frequency: the increase of the input waveguide diameter or the use of the coaxial input. If the maximum input power level is not so high, the calorimeter dimensions can also be minimized. The problem of feasibility of this design at higher frequencies is mostly reduced to the choice of materials with required properties, such as an absorbing liquid and a dielectric material that parts liquid and vacuum volumes.

4. CONCLUSION

The novel design of ultra-wideband liquid based calorimeter was proposed. The proof of concept was demonstrated by numerical simulation and optimization of the design for the frequency band from X- to Ka-bands. Ethanol was used as an absorbing medium. The frequency dependence of its dielectric constant was incorporated in the simulation model. The accepted power level is of the order of hundreds of megawatts. Supposed operating modes are symmetrical TM_{0n} ones. The reflection coefficient for TM_{01} mode is below -20 dB at lowest frequency of 8 GHz and well below the level of -25 dB from 10 to 38 GHz. The reflection coefficients for higher order modes are below -30 dB until the operating frequency is close to the cut-off frequency for a particular mode. The sensitive point for a calorimeter user is a design of the transition from a microwave source output to the calorimeter input, as the maximum accepted power levels may differ four times for specific mode mixtures.

This design can be scaled up to accept more input power and/or to lower the minimal operating frequency. If the maximum input power is lower than we predefined, the transverse dimensions can be reduced to about the size of standard waveguide for the lowest operating frequency. Moreover, this design could be easily transformed to a coaxial input of microwave power, so it might greatly extend its usage in lower frequency bands.

ACKNOWLEDGMENT

This work was supported by the Russian Foundation for Basic Research (RFBR): grant 18-42-700012-p.a.

REFERENCES

1. Benford, J., J. A. Swegle, and E. Shamiloglu, *High Power Microwaves*, Taylor & Francis, Oxford, 2007.
2. Huttlin, G. A., et al., "The reflex-diode HPM source on Aurora," *IEEE Trans. Plasma Sci.*, Vol. 18, No. 3, 618–625, 1990.
3. Bugaev, S. P., et al., "Relativistic multiwave cerenkov generators," *IEEE Trans. Plasma Sci.*, Vol. 18, No. 3, 525–536, 1990.
4. Efthimion, P., P. R. Smith, and S. P. Schlesinger, "Broad spectral electromagnetic radiation calorimeter: Centimeters to microns," *Rev. Sci. Instrum.*, Vol. 47, No. 9, 1059–1062, 1976.
5. Warton, C. B., L. M. Earley, and W. P. Ballard, "Calorimetric measurements of single-pulse high-power microwaves in oversized waveguides," *Rev. Sci. Instrum.*, Vol. 57, No. 5, 855–858, 1986.
6. Earley, L. M., W. P. Ballard, and L. D. Roose, "Rectangular waveguide calorimeter for single intense microwave pulses," *Rev. Sci. Instrum.*, Vol. 57, No. 9, 2359–2361, 1986.

7. Earley, L. M., et al., "Comprehensive approach for diagnosing intense single-pulse microwave sources," *Rev. Sci. Instrum.*, Vol. 57, No. 9, 2283–2293, 1986.
8. Zaitsev, N. I., et al., "A calorimeter for measuring the energy of a high-power electromagnetic pulse," *Instrum. Exp. Tech.*, Vol. 35, No. 2, 283–284, 1992.
9. Belousov, V. I., et al., "Calorimeter for measuring the total energy of high-power pulse millimeter-range devices," *Instrum. Exp. Tech.*, Vol. 39, No. 3, 402–405, 1996.
10. Belousov, V. I., et al., "A dry overmoded-waveguide calorimeter for measurement of high-power microwave pulse energy," *Instrum. Exp. Tech.*, Vol. 35, No. 3, 482–487, 1992.
11. Bykov, N. M., et al., "Diagnosis of high-power nanosecond pulses of microwave-radiation," *Instrum. Exp. Tech.*, Vol. 30, No. 6(2), 1393–1397, 1987.
12. Klimov, A. I., et al., "A calorimeter for high power microwave pulse measurement," *Proceedings of 15th International Symposium on High Current Electronics*, 422–424, Tomsk, Russia, 2008.
13. Lisichkin, A. L. and E. V. Nesterov, "Waveguide calorimeter for pulsed microwave radiation in the centimeter wavelength range," *Instrum. Exp. Tech.*, Vol. 41, No. 3, 362–364, 1998.
14. Kiselev, V. A., et al., "A calorimeter with a capacitive probe for measuring microwave energy," *Instrum. Exp. Tech.*, Vol. 48, No. 2, 230–233, 2005.
15. Lisichkin, A. L., E. V. Nesterov, and V. A. Stroganov, "Calorimeter for pulsed microwave radiation," *Instrum. Exp. Tech.*, Vol. 39, No. 1, 70–72, 1996.
16. Shkvarunets, A. G., "A broadband microwave calorimeter of large cross section," *Instrum. Exp. Tech.*, Vol. 39, No. 4, 535–538, 1996.
17. Lisichkin, A. L., et al., "A liquid pulsed microwave radiation calorimeter," *Instrum. Exp. Tech.*, Vol. 50, No. 1, 82–85, 2007.
18. Klimov, A. I., et al., "Measurement of parameters of X-band high-power microwave super radiative pulses," *IEEE Trans. Plasma Sci.*, Vol. 36, No. 3, 661–664, 2008.
19. Vykhodtsev, P. V., et al., "Liquid calorimeters for measuring the energy of high-power microwave pulses," *Instrum. Exp. Tech.*, Vol. 58, No. 4, 510–514, 2015.
20. Teng, Y., et al., "High-efficiency coaxial relativistic backward wave oscillator," *Rev. Sci. Instrum.*, Vol. 82, No. 2, 024701, 2011.
21. Ye, H., et al., "Research on calorimeter for high-power microwave measurements," *Rev. Sci. Instrum.*, Vol. 86, No. 12, 124706, 2015.
22. Klimov, A. I. and V. Yu. Kozhevnikov, "Numerical optimization of aperture absorbing loads of liquid calorimeters for high-power microwave pulses," *Rus. Phys. Journ.*, Vol. 60, No. 8, 1319–1324, 2017.
23. Dagys, M., et al., "The resistive sensor: A device for high-power microwave pulsed measurements," *IEEE Antennas and Propagation Magazine*, Vol. 43, No. 5, 64–79, 2001.
24. Ballard, W. P. and L. M. Earley, "Microwave detecting diode rise-time measurements," *Rev. Sci. Instrum.*, Vol. 56, No. 7, 1470–1472, 1985.
25. Lobaev, M. A., et al., "Effect of inhomogeneous microwave field on the threshold of multipactor discharge on a dielectric," *Tech. Phys. Lett.*, Vol. 35, No. 12, 1074–1077, 2009.
26. Chang, C., et al., "The effect of grooved surface on dielectric multipactor," *J. Appl. Phys.*, Vol. 105, No. 12, 123305, 2009.
27. Klimov, A. I. and E. M. Totmeninov, "Diffraction effects in measurements of characteristics of high-power microwave pulses with wide aperture liquid calorimeters," *Rus. Phys. Journ.*, Vol. 60, No. 6, 964–971, 2017.
28. Tarakanov, V. P., et al., "Time-dependent numerical simulation of diffraction and absorption effects in diagnostics of short high-power microwave pulses using wide-aperture liquid calorimeters," *EPJ Web Conf.*, Vol. 149, 04046, 2017.
29. ANSYS HFSS 3D Electromagnetic Field Simulator for RF and Wireless Design [online] available at <https://www.ansys.com/products/electronics/ansys-hfss>.
30. Schamiloglu, E., et al., "High-power microwave-induced TM/sub01/plasma ring," *IEEE Transactions on Plasma Science*, Vol. 24, No. 1, 6–7, 1996.

31. Ivanov, O. A., M. A. Lobaev, V. A. Isaev, and A. L. Vikharev, "Experimental study of a multipactor discharge on a dielectrics surface in a high- Q microwave cavity," *Plasma Phys. Reports*, Vol. 36, No. 4, 336–344, 2010.
32. Lobaev, M. A., et al., "Effect of inhomogeneous microwave field on the threshold of multipactor discharge on a dielectric," *Tech. Phys. Lett.*, Vol. 35, No. 12, 1074–1077, 2009.
33. Krupka, J., "Measurements of the complex permittivity of low loss polymers at frequency range from 5 GHz to 50 GHz," *IEEE Microw. Wireless Compon. Lett.*, Vol. 26, No. 6, 464–466, 2016.
34. Bao, J., M. L. Swicord, and C. C. Davis, "Microwave dielectric characterization of binary mixtures of water, methanol, and ethanol," *J. Chem. Phys.*, Vol. 104, No. 12, 4441–4450, 1996.
35. Barthel, J. K. Bachhuber, R. Buchner, and H. Hetzenauer, "Dielectric spectra of some common solvents in the microwave region. Water and lower alcohols," *Chem. Phys. Lett.*, Vol. 165, No. 4, 369–373, 1990.
36. Sato, T. and R. Buchner, "Dielectric relaxation processes in ethanol/water mixtures," *J. Phys. Chem. A*, Vol. 108, No. 23, 5007–5015, 2004.
37. "Agilent basics of measuring the dielectric properties of materials. Application note," *Agilent Technologies*, 2013.
38. Cole, K. S. and R. H. Cole, "Dispersion and absorption in dielectrics. I. Alternating current characteristics," *J. Chem. Phys.*, Vol. 9, 341–352, 1941.